Journal for ImmunoTherapy of Cancer

KLRG1 marks tumor-infiltrating CD4 T cell subsets associated with tumor progression and immunotherapy response

Casey R Ager ,[1,2,3,4] Mingxuan Zhang,[1,5] Matthew Chaimowitz,[3,6] Shruti Bansal,[3,6] Somnath Tagore,[1,7] Aleksandar Obradovic,[1,7] Collin Jugler,[2] Meri Rogava,[1,3] Johannes C Melms,[1,3] Patrick McCann,[3,6] Catherine Spina,[3,6] Charles G Drake,[1,3,4,8,9] Matthew C Dallos,[1,9,10] Benjamin Izar [1,3,7,9,11]

To cite: Ager CR, Zhang M, Chaimowitz M, *et al*. KLRG1 marks tumor-infiltrating CD4 T cell subsets associated with tumor progression and immunotherapy response. *Journal for ImmunoTherapy of Cancer* 2023;**11**:e006782. doi:10.1136/jitc-2023-006782

► Additional supplemental material is published online only. To view, please visit the journal online (http://dx.doi.org/10.1136/jitc-2023-006782).

Accepted 08 August 2023

For numbered affiliations see end of article.

Correspondence to
Dr Casey R Ager;
ager.casey@mayo.edu

Dr Benjamin Izar;
bi2175@cumc.columbia.edu

ABSTRACT

Current methods for biomarker discovery and target identification in immuno-oncology rely on static snapshots of tumor immunity. To thoroughly characterize the temporal nature of antitumor immune responses, we developed a 34-parameter spectral flow cytometry panel and performed high-throughput analyses in critical contexts. We leveraged two distinct preclinical models that recapitulate cancer immunoediting (NPK-C1) and immune checkpoint blockade (ICB) response (MC38), respectively, and profiled multiple relevant tissues at and around key inflection points of immune surveillance and escape and/or ICB response. Machine learning-driven data analysis revealed a pattern of KLRG1 expression that uniquely identified intratumoral effector CD4 T cell populations that constitutively associate with tumor burden across tumor models, and are lost in tumors undergoing regression in response to ICB. Similarly, a Helios^{-}KLRG1^{+} subset of tumor-infiltrating regulatory T cells was associated with tumor progression from immune equilibrium to escape and was also lost in tumors responding to ICB. Validation studies confirmed KLRG1 signatures in human tumor-infiltrating CD4 T cells associate with disease progression in renal cancer. These findings nominate KLRG1^{+} CD4 T cell populations as subsets for further investigation in cancer immunity and demonstrate the utility of longitudinal spectral flow profiling as an engine of dynamic biomarker discovery.

BACKGROUND

Immunotherapy is now a pillar of cancer treatment. However, responses to most immunotherapeutic agents remain rare, restricted to a limited number of tumor types, and difficult to predict.[1] Improving response rates and developing biomarkers predictive of response are central goals of the tumor immunology field, but this remains challenging. A multitude of complex multicellular interactions may govern the outcome of an antitumor immune response in any given patient. Therefore, it is common that single biomarkers—or therapeutic modulation of singular pathways—tend to have utility in some, but not most patients with cancer.

For example, there are three immune-related biomarkers currently in widespread clinical use: (1) tumor mutational burden, as measured directly or inferred via the presence of disabling mutations in DNA repair machinery,[2–4] (2) PD-L1 expression by immunohistochemistry,[5] and (3) pre-existing immunity as measured by the presence of CD8 T cells within and surrounding tumors, termed the Immunoscore.[6]

While each is significantly associated with response to immunotherapy in certain contexts, the sensitivity and specificity of these predictors remain suboptimal.[7] Many additional biomarkers are under investigation, including frequencies of immunosuppressive cell types such as myeloid derived suppressor cells and regulatory T cells (Tregs), or spatial 'neighborhoods' of immune populations such as tertiary lymphoid structures, which associate with immunotherapy response.[7 8] Nevertheless, these approaches likely fail to fully capture the complex mechanisms underlying antitumor immunity, particularly the dynamic nature of such responses occurring across tissues and over time. As such, application of highly multiplexed single cell immune profiling approaches to biomarker detection and target discovery in a cross-tissue, longitudinal manner may provide nuanced immune phenotypes with greater predictive and translational utility.

To this end, we developed a 34-parameter spectral flow cytometry panel and high dimensional data analysis pipeline to interrogate protein-level immune phenotypes associated with different phases of the cancer

immunoediting cycle, including immune escape and tumor outgrowth, and immune checkpoint blockade (ICB) response across preclinical models. We profiled the NPK-C1 and ICB-treated MC38 models, analyzing multiple tissues (tumor, draining vs non-draining lymph nodes, and blood) over and around key inflection points in tumor progression. This facilitated deep characterization of dynamics underlying natural and ICB-induced tumor regression, transition to immune equilibrium, and subsequent transition from equilibrium to uncontrolled tumor escape. Validation studies in human single cell datasets of renal cancer confirmed the translational relevance of these findings.

METHODS

Mice

Male and female C57BL/6J mice (5–6 weeks old) were purchased from the Jackson Laboratory (Bar Harbor, Maine, USA). Mice were 6–8 weeks old at time of use. All animals were housed in strict accordance with NIH and American Association of Laboratory Animal Care regulations.

Cell lines

The NPK-C1 cell line (originally LM7304) was provided by Dr. Cory Abate-Shen at Columbia University. See prior references for further detail.[9 10] NPK-C1 cells were maintained in R10, consisting of RPMI medium (Corning; Corning, New York, USA) supplemented with 10% FBS (fetal bovine serum; HyClone; Logan, Utah, USA), 100 U/mL penicillin, and 100 mg/mL streptomycin (Gibco; Gaithersburg, Maryland, USA). NPK-C1 cells were authenticated using the MiniMUGA genotyping array through Transnetyx (Cordova, Tennessee, USA). MC38 colon carcinoma cells were purchased from Kerafast and cultured in D10 consisting of DMEM (Dulbecco's Modified Eagle Medium; Corning; Corning, New York, USA) supplemented with 10% FBS, 100 U/mL penicillin, and 100 mg/mL streptomycin (Gibco; Gaithersburg, Maryland, USA). MC38 was authenticated by Kerafast, and cells were used for experiments within four passages of original purchase.

Tumor challenge and therapy injections

NPK-C1 cells at 70%–90% confluence or MC38 cells at 50%–75% confluence were harvested with 0.05% trypsin (Gibco), washed with PBS, counted, and resuspended at 10×10^6 cells/mL in ice cold PBS. On day 0, mice aged 6–8 weeks were implanted on the right flank with 1×10^6 NPK-C1 (male mice) or MC38 (female mice) cells. Cages were assigned randomly to treatment groups. Tumor measurements were recorded in X, Y, and Z dimensions in a non-blinded fashion (largest diameter, smallest diameter, and largest height, respectively) every 2–3 days by digital caliper and tumor volume was calculated by multiplying X*Y*Z. Anti-PD-1 (*RMP1-14* IgG2a,κ) or Rat IgG2a isotype antibody (Bio X Cell; Lebanon, New Hampshire, USA) was diluted in sterile PBS and administered by intraperitoneal injection at 200 µg/mL per mouse on days 3, 6, 9, and 12 post-MC38 implantation. Tumor measurements and treatments were administered by different researchers to reduce potential confounding variables and/or bias.

Tissue harvesting

Following mouse euthanasia, ~200 µL blood was isolated via cardiac puncture using a 0.2% heparin (StemCell Technologies; Vancouver, BC) coated syringe needle and placed on ice in tubes containing 10 µL 0.5M EDTA (Corning; Corning, New York, USA). Tumor-draining and non-draining inguinal lymph nodes (TDLN/NDLN) were dissected and placed in 48-well plates containing 150 µL R10 media on ice. Tumors were harvested, massed, and up to 50 mg tumor was diced and placed in X-Vivo 15 media (Lonza; Basel, Switzerland) in 5 mL Eppendorf tubes on ice. DNase (40 µL of 20 mg/mL solution; Roche; Basel, Switzerland) and Collagenase D (125 µL of 40 mg/mL solution; Roche; Basel, Switzerland) were added to tumor samples prior to incubation on a shaker at 37°C for 30 min. Digest reactions were quenched by vortexing (30 s) and adding 5mL R10 media. Tumor digest was filtered through 70 µm filters (Miltenyi; Bergisch Gladbach, GE) and pelleted. Blood samples were RBC lysed with two successive 2 min incubations in 2 mL ACK buffer (Quality Biological; Gaithersburg, Maryland, USA) and quenching in R10 prior to pelleting. Lymph nodes were physically disaggregated with a 1 mL syringe plunger in the 48-well plate, then suspensions were filtered through 40 µm filters. All samples were placed in U-bottom 96-well plates for staining.

Flow cytometry

Samples were washed with PBS. Dead cells were stained by resuspension in 100 µL PBS+Live/Dead Fixable Blue dye (1:500; Invitrogen; Waltham, Massachusetts, USA). This and all further staining or fixation steps were performed for 30 min at room temperature on a plate shaker, protected from light. Samples were washed 2× with PBS, then were resuspended in FACS (PBS+3% FBS+1 mM EDTA+10 mM HEPES) supplemented with TruStain FcX (1:50; BioLegend; San Diego, California, USA) and TruStain Monocyte Blocker (1:20; BioLegend) and placed on ice. Surface antibodies were prepared at optimal dilutions (see online supplemental table S1) in FACS supplemented with Brilliant Stain Plus buffer (BD; Franklin Lakes, New Jersey, USA), then were added to samples in blocking solution. After staining, samples were washed 2× with FACS buffer and fixed in 100 µL of FoxP3 Fixation/Permeabilization Kit buffer (eBioscience; San Diego, California, USA). Samples were washed twice with 1X Permeabilization buffer (1X PW) then were stained in 1X PW plus intracellular antibodies. Samples were then washed twice in 1X PW then fixed in 100 µL of FluoroFix buffer (BioLegend), washed twice with FACS, then resuspended in 200 µL FACS and sealed in the 96-well plate for

acquisition the following day on a Cytek Aurora 5-laser cytometer. Simultaneously stained splenocyte samples were used for single stain controls.

Analysis and statistics

Longitudinal profiling experiments were conducted once each for MC38 and NPK-C1 models. A total of n=10 mice per time point were evaluated except for D24 in the NPK-C1 model, where n=25 mice were evaluated as was previously required for optimal power in the NPK-C1 model.[8] All mice with tumors of sufficient size to be harvested were included in the analysis. Flow cytometry data was analyzed in FlowJo V.10.8.1 (BD; Franklin Lakes, New Jersey, USA) and high dimensional plugin algorithms UMAP and FlowSOM were downloaded from FlowJo Exchange. Up to 30k live CD45$^+$ tumor-infiltrating cells and up to 15k live CD45$^+$ blood or LN-derived cells per sample were concatenated for high dimensional analysis. All dimensionality reduction and clustering were performed in FlowJo. Statistical analyses were performed in GraphPad Prism V.9.3.1. Pearson correlation was used to generate correlation coefficients, and unpaired Student's t-tests with Welch's correction were used to compare cluster frequencies between groups. Outliers were identified by ROUT method with Q=0.1%, the most stringent value to identify only definitive outliers. Single cell analytical methods are previously described.[11 12] The KLRG1 regulon was extracted from the consensus metaVIPER KLRG1 regulon from Obradovic *et al*.[12] To compute the KLRG1 regulon signature, we fit a random forest regression model with regulons genes as features and KLRG1 as target, then computed Gini importance scores of regulon genes to determine their impact on KLRG1 expression. The KLRG1 regulon score of each cell was given by the weighted sum of expression measures of all regulon genes in the cell with importance scores as weights.

RESULTS

Longitudinal profiling captures generalizable features of failed versus successful antitumor immunity

We generated a 34-parameter spectral flow cytometry panel (see list of antibodies used in online supplemental table S1 and additional clustering in online supplemental figure S1) to profile productive versus non-productive immunity in NPK-C1 (derived from *Nkx3.1*$^{CreERT2/+}$; *Pten*$^{flox/flox}$; *Kras*$^{LSL\text{-}G12D/+}$; *R26R*-$^{LSL\text{-}YFP/+}$ mice), a prostate cancer model known to undergo spontaneous immunoediting in native C57BL/6 hosts,[9] and the well-characterized carcinogen-induced MC38 colorectal cancer model (C57BL/6 syngeneic) treated with curative doses of anti-PD-1 immunotherapy (figure 1A). Specifically, we profiled days 7, 10, and 13 postimplantation of NPK-C1 and MC38, and additional days 20 and 24 of NPK-C1 (representing the equilibrium to escape transition). We used a rigorous high dimensional analysis pipeline improved on a previous study[9] with minimally supervised UMAP (uniform manifold approximation projection) dimensionality reduction and FlowSOM clustering algorithms to establish cellular identities in high dimensional space (see online supplemental figure S1A–E for analysis workflow).

KLRG1 accumulates selectively on tumor-infiltrating CD4 T cell subsets

We observed diverse phenotypic heterogeneity in tumor-infiltrating Tregs infiltrating both NPK-C1 and MC38 tumors (figure 1B, online supplemental figure S1B,C). In both models, we observed a dynamic shift in these phenotypes as tumors progressed. At late time points, up to 80% of Tregs existed in clusters marked by expression of KLRG1 (figure 1B,C). We observed a similar phenotypic trajectory in the FoxP3$^-$ Tconv compartment, as KLRG1 expression defined a distinct Tconv cluster accounting for up to 50%–70% of tumor Tconv at late time points in NPK-C1 and MC38, respectively. Phenotypic analysis of KLRG1$^+$ versus KLRG1$^-$ clusters from both tumor models indicated a consistent coexpression pattern of KLRG1 with high levels of CD39 and ICOS on both tumor-infiltrating Tregs and Tconv (figure 1D). In contrast, ST2/IL-33R, CD69, and CD103 were present on subsets of both KLRG1$^+$ and KLRG1$^-$ Tregs and Tconv (figure 1D), suggesting KLRG1 marks CD4 cell states independent of tissue residence programming or IL-33 signaling, as has been reported.[13]

To determine whether KLRG1 is selectively induced on tumor-infiltrating CD4 T cells during tumor progression, we measured expression of KLRG1 on other immune subsets as well as CD4 T cells in the tumor, TDLN and NDLN and blood (figure 1E–H). KLRG1 expression peaked early on CD8 and NK cells infiltrating both NPK-C1 and MC38 tumors, in contrast to CD4 Tconv and Tregs where KLRG1 expression increased over time (figure 1E). KLRG1 was expressed by 5%–10% of Tregs in both TDLNs and NDLNs, and throughout tumor progression a moderate trend toward an increase in KLRG1$^+$ Tregs was observed in the TDLN, but not the NDLN (figure 1F,G). NK cells were the only other subset to express KLRG1 in LNs, however, this expression did not increase with tumor progression. In the blood, KLRG1 was expressed on subsets of CD8s, Tregs, Tconv, and NK cells, however, the frequency of cells expressing KLRG1 in each compartment did not correlate with time of tumor progression (figure 1H). Together, these data reveal a tumor model-independent and TME-restricted phenomenon in which CD4 T cell subsets uniquely gain increasing levels of KLRG1 expression throughout tumor progression.

Lack of tumor KLRG1$^+$ Tconv associates with enhanced tumor control

Based on these data, we next asked whether KLRG1 expression on tumor CD4 T cells has utility as a biomarker of tumor burden or ICB response. We first generated Pearson correlation coefficients for all predominant

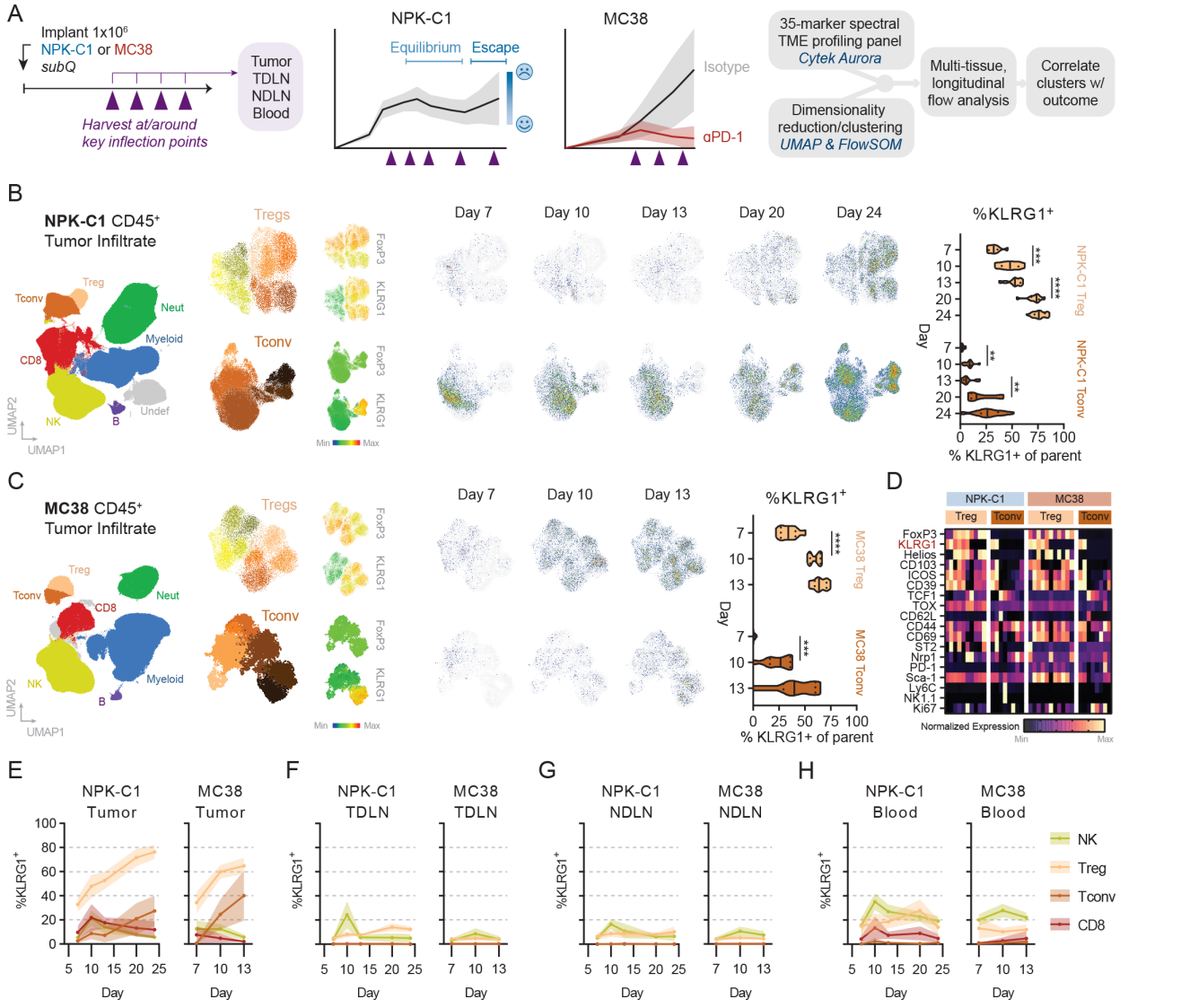

Figure 1 Expression of KLRG1 on tumor-infiltrating CD4 T cells over time in MC38 and NPK-C1. (A) Schematic summary of study design, models used, and analysis pipeline. (B) Dimensionality reduction (UMAP) and clustering (FlowSOM) of NPK-C1 (B) and MC38 (C) infiltrating immune cells, focusing on CD4$^+$ Treg and Tconv populations. Cell-type subclustering, expression of FoxP3 and KLRG1 by heat map coloring, UMAP time courses, and frequencies of KLRG1 expression in each cell type. (D) Expression of phenotypic markers on all CD4 T cell sub-clusters across NPK-C1 and MC38 markers. Color scale is normalized to min/max of the cell type or all immune cells, as appropriate. Quantitation of KLRG1 expression in other immune cell types in the tumor (E) TDLN (F), NDLNs (G), and blood (H). Data were generated from one experiment of n=10–25 mice per/condition and time point. Statistical significance is denoted by **p<0.01, ***p<0.001, ****p<0.0001. NDLNs, non-draining lymph nodes; TDLN, tumor-draining lymph node.

immune phenotypes in the TME across time points and both treatment-naïve models (figure 2A). We manually curated these phenotypes into 22 immune metaclusters by grouping FlowSOM-derived subpopulations sharing a dominant subphenotypic marker. While the majority of clusters varied in association with tumor burden over time and across models, KLRG1$^+$ Tconv were strikingly consistent in their correlation with increased tumor burden at every time point in both NPK-C1 and MC38 (figure 2A,B). On day 24, NPK-C1 tumors either begin progressing to immune escape or stay under immune-regulated equilibrium, allowing assessment of cell types implicated in the poorly understood but clinically relevant equilibrium-to-escape transition (figure 2C).[9] Of note, KLRG1$^+$ Tconv cells were highly enriched in NPK-C1 tumors escaping immune control (figure 2D–E; n=7 of 25 tumors escaped). These associations would suggest KLRG1$^+$ Tconv possess a tumor-supportive role in the treatment-naïve setting. To determine whether KLRG1$^+$ Tconv also associate with response to ICB, we compared frequencies of KLRG1$^+$ Tconv in MC38-bearing mice undergoing progressive growth versus those undergoing curative responses to anti-PD-1 (figure 2F). While KLRG1 expression was rare on CD4 Tconv on day 7, we observed a significant decrease in KLRG1$^+$ Tconv cells in anti-PD-1 treated animals on both day 10 (p=0.014) and day 13

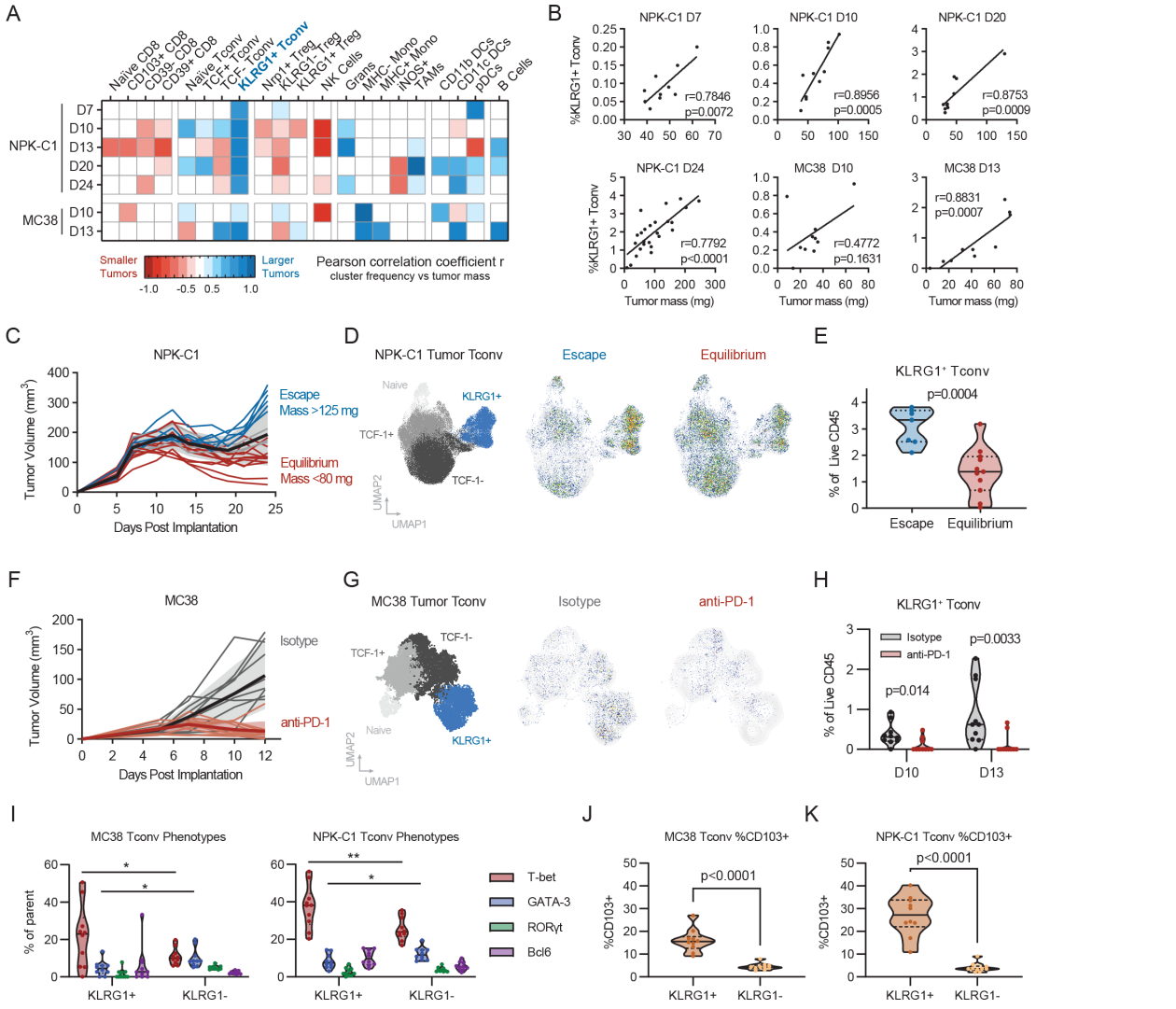

Figure 2 Association between KLRG1$^+$ Tconv frequency and tumor progression. (A) Heatmap of Pearson correlation coefficients comparing metacluster frequency (% of CD45) versus tumor mass. (B) Dot plots of selection correlations as shown in (A). (C) Schematic of NPK-C1 model with colors representing escaping tumors (>125 mg) versus those remaining in equilibrium (<80 mg) on D24. (D) UMAP projections of CD4 Tconv metaclusters and pseudocolor representations of cells from escape tumors versus equilibrium tumors. (E) Violin plot of KLRG1$^+$ Tconv frequency in escape versus equilibrium tumors. (F) Schematic of MC38 model. (G) UMAP projections of CD4 Tconv metaclusters and pseudocolor representations of cells from isotype versus anti-PD-1 treated tumors. (H) Violin plot of KLRG1$^+$ Tconv frequency in isotype versus anti-PD-1 tumors on day 10 and day 13. (I) Expression of T helper subset transcription factors in KLRG1$^+$ and KLRG1$^-$ Tconv in MC38 and NPK-C1 tumors by flow cytometry. (J) Expression of CD103 on KLRG1$^+$ and KLRG1$^-$ Tconv infiltrating MC38 and (K) NPK-C1 tumors. Data were generated from one experiment of n=10–25 mice per/condition and time point. Statistical significance is denoted by *p<0.05, **p<0.01.

(p=0.0033; figure 2H) as compared with isotype treated animals. To understand the polarization status of KLRG1$^+$ Tconv, we assessed expression of canonical helper T cell lineage-defining transcription factors by flow cytometry. We found that KLRG1$^+$ Tconv in both MC38 and NPK-C1 models can belong to any lineage (Th1, Th2, Th17, or Tfh), however, KLRG1$^+$ Tconv are most enriched for the Th1 (T-bet$^+$) phenotype as compared with KLRG1$^-$ Tconv (figure 2I). Independent of lineage, we also found KLRG1$^+$ Tconv to possess a resident memory-like phenotype via expression of CD103 and CD69 (figure 2J,K, figure 1D). In total, these data indicate tumor-resident Th1-like KLRG1$^+$ Tconv frequencies associate consistently with tumor burden over multiple time points throughout tumor progression and across distinct models, and may have unappreciated functional roles in the TME or utility as biomarkers of response to immunotherapy.

Tumor Helios$^-$KLRG1$^+$ Treg deficiency associates with enhanced tumor control

Based on these findings, we also investigated whether KLRG1$^+$ Treg phenotypes associate with tumor progression or ICB response. While KLRG1$^+$ Tregs as a bulk population did not correlate consistently with tumor burden in the NPK-C1 or MC38 models (figure 2A), we observed two Treg subclusters defined by Helios$^-$KLRG1$^+$

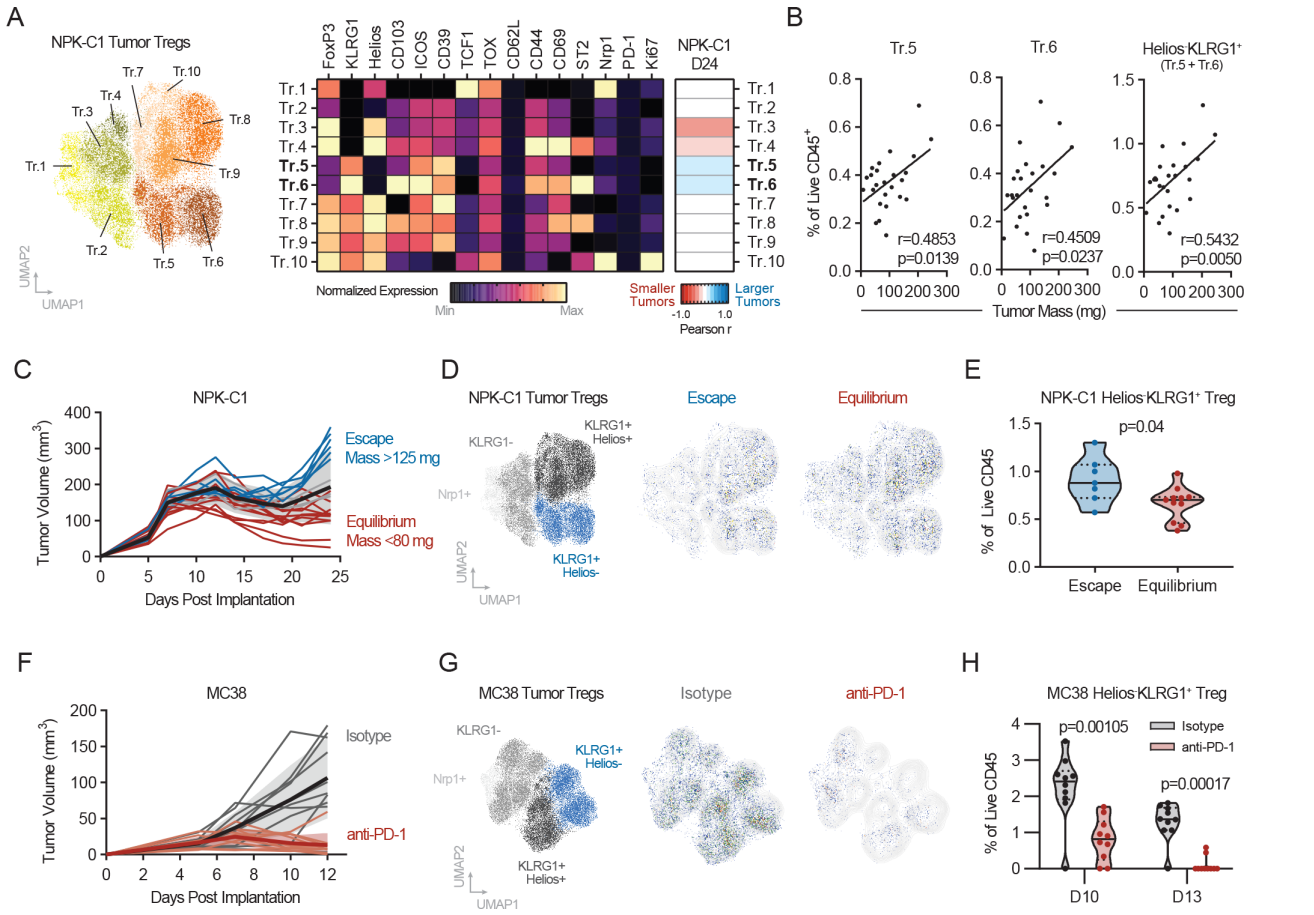

Figure 3 Association between Helios$^-$KLRG1$^+$ Treg frequency and tumor progression. (A) UMAP projection and FlowSOM clustering of NPK-C1 tumor Tregs, and cluster heatmap of normalized phenotypic marker expression. Pearson correlation of each cluster frequency versus tumor mass shown by heat map, and selected correlation dot plots in (B). (C) Schematic of NPK-C1 model with colors representing escaping tumors (>125 mg) versus those remaining in equilibrium (<80 mg) on D24. (D) UMAP projections of CD4 Treg metaclusters and pseudocolor representations of cells from escape tumors versus equilibrium tumors. (E) Violin plot of Helios$^-$KLRG1$^+$Treg frequency in escape versus equilibrium tumors. (F) Schematic of MC38 model. (G) UMAP projections of CD4 Treg metaclusters and pseudocolor representations of cells from isotype versus anti-PD-1-treated tumors. (H) Violin plot of Helios$^-$KLRG1$^+$Treg frequency in isotype versus anti-PD-1 tumors on day 10 and day 13. Data were generated from one experiment of n=10–25 mice per/condition and time point.

that correlated significantly with tumor burden on day 24 in the NPK-C1 model, which indicates an association between this Treg phenotype and transition of NPK-C1 tumors from equilibrium to escape (figure 3A–E). To test the generalizability of this Treg phenotype and its functional associations across models, we asked whether the Helios$^-$KLRG1$^+$ Treg phenotype is associated with curative responses to immunotherapy in MC38 (figure 3F). FlowSOM clustering produced two Helios$^-$KLRG1$^+$ Treg clusters that were present in progressive untreated tumors, but were significantly lost on day 10 (p=0.001) and day 13 (p=0.00017; figure 3H) in anti-PD-1 treated animals. Therefore, the Helios$^-$ subset of KLRG1$^+$ Tregs exhibits relevant associations with disease progression and response to ICB in distinct tumor models, suggesting a potentially generalizable role for Helios$^-$KLRG1$^+$ Tregs in tumor immunity and response to immunotherapy.

KLRG1$^+$ CD4 T cells correlate with tumor progression in kidney cancer

To validate the translational relevance of our findings, we asked whether KLRG1 in human tumor-infiltrating T cells associates with clinical disease progression. For this, we analyzed data from two cohorts of clear cell renal carcinoma (ccRCC) patients whose tumors were profiled by single cell RNA sequencing.[11 12] At the gene expression level, *KLRG1* is present largely in CD8 T cells as well as CD4 and NK cells (figure 4A). However, we inferred KLRG1 protein activity by VIPER (Virtual Inference of Protein activity by Enriched Regulon analysis; see references 12 14 for validation of method) and found by contrast that KLRG1 inferred protein activity is highest in CD4 Tconv in RCC tumors (figure 4B). KLRG1 protein activity is significantly increased in Tconv infiltrating ccRCC as compared with Tconv in adjacent normal kidney parenchema, further validating the relevance of the KLRG1$^+$ CD4 T cell phenotype in human cancer (p=1.40e–102; figure 4C).

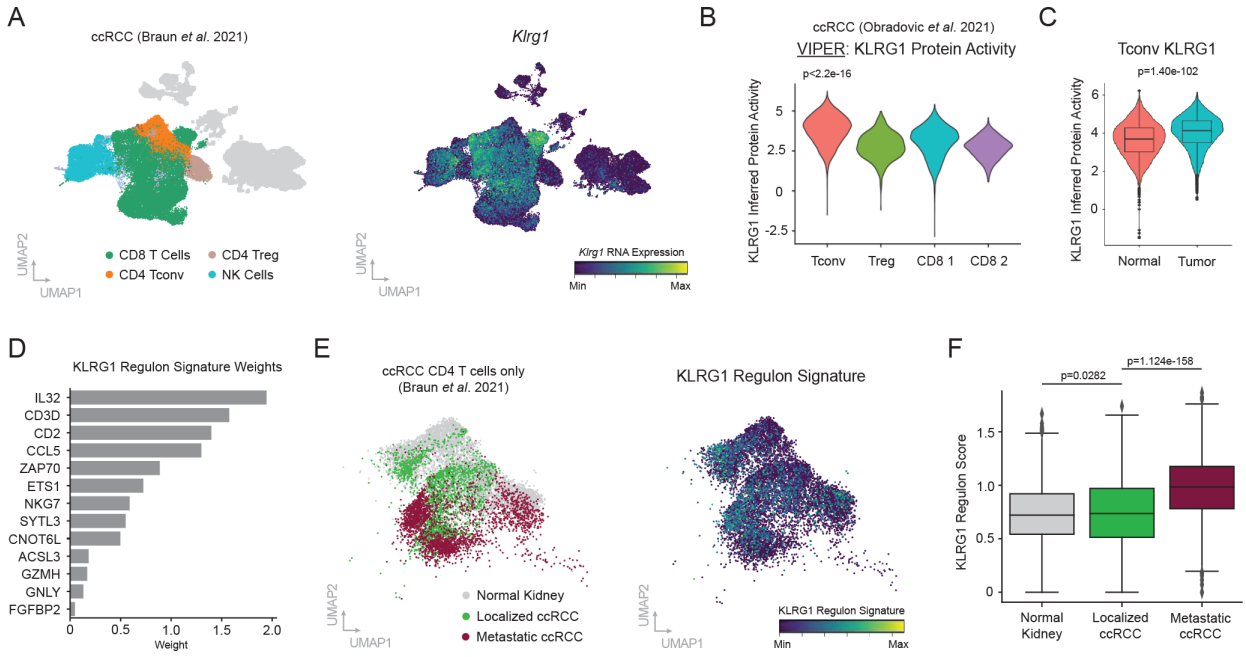

Figure 4 Validation of KLRG1$^+$ Tconv association with tumor progression in human RCC. (A) UMAP projection of ccRCC single cell data from Braun *et al.*[11] *Klrg1* gene expression is shown. (B) VIPER inferred protein activity of KLRG1 in ccRCC T cell populations from Obradovic *et al.*[12] (C) Inferred activity of KLRG1 in CD4 Tconv in ccRCC tumors versus adjacent normal kidney. (D) Bar plot of gene weights learned by random forest regression for KLRG1 regulon signature scor(E) UMAP projection of ccRCC CD4 T cells from Braun *et al.*[11] KLRG1 signature score is shown. (F) Quantification of KLRG1 regulon score in CD4 T cells in normal kidney versus localized ccRCC versus metastatic ccRCC. ccRCC, clear cell renal cell carcinoma.

To test whether KLRG1 activity in CD4 Tconv associates with disease progression, we computed a KLRG1 regulon signature consisting of genes whose upregulation at the RNA level predicts KLRG1 protein activity (figure 4D), then asked whether this KLRG1 signature is enriched in CD4 Tconv infiltrating late-stage versus early-stage ccRCC. For this, we focused on the Braun dataset as it was generated to profile T cell phenotypes across stages of ccRCC progression.[11] We found the KLRG1 regulon signature score increased from naïve kidney to localized ccRCC (p=0.0282), and was highly enriched in metastatic disease (p=1.124e–158; figure 4E,F). These data validate our preclinical flow cytometry observations and warrant additional mechanistic and validation studies to understand the utility of tumor-infiltrating KLRG1$^+$ CD4 T cell phenotypes as biomarkers and/or targets of cancer immunotherapy.

DISCUSSION

In this study, we generated a comprehensive spectral flow cytometry dataset of productive versus non-productive immunity across tissues and relevant time points in the NPK-C1 and MC38 murine tumor models. Using dimensionality reduction and minimally supervised clustering analyses, we identified subphenotypes of tumor-infiltrating CD4 Tregs and Tconv cells marked by KLRG1 expression, whose relative frequencies associate with tumor burden, tumor progression from equilibrium to escape, and response to anti-PD-1 immunotherapy.

CD4 T cells expressing KLRG1 have been previously discovered in both murine and human tumors, yet the etiology and functional properties of these cells remain incompletely described.[15 16] Canonically, KLRG1 is a coinhibitory receptor expressed on T cells and NK cells typically considered a marker of terminal differentiation and/or senescence owing to its negative regulation of TCR and Akt signaling and its positive effects on cell cycle checkpoints p16^{ink4a} and p27^{kip1}.[15] In a related study by Li *et al*, KLRG1$^+$Amphiregulin$^+$ Tregs were shown by single cell RNA sequencing and flow cytometry to accumulate in autochthonous Kras^{G12D} p53$^{-/-}$ (KP)-driven lung tumors. These Tregs were driven by IL-33 signaling, thus Treg-conditional ablation of ST2/IL-33R reduced KLRG1$^+$ Treg frequency and derepressed CD8 T cell mediated antitumor immunity.[13] While our data do not disqualify a role for IL-33 in inducing KLRG1$^+$ Tregs or Tconv cells in our models, we note that ST2/IL-33R expression was not characteristic of or restricted to KLRG1$^+$ CD4 T cells in our data. It remains possible other tissue factors such as TGF-β contribute to the KLRG1$^+$ Treg or Tconv in the TME, as observed in the intestinal environment.[17] Our data support previous observations that KLRG1$^+$ Tregs and Tconv exhibit an activated, terminally differentiated phenotype expressing high levels of CD39 and ICOS.[18 19] While our correlative data suggest these phenotypes are tumor-supportive, additional studies are warranted to determine the mechanisms by which this occurs.

For KLRG1$^+$ Tconv, it is possible that these cells are exhausted, analogous to a KLR$^+$ exhausted CD8 T cell program described in the chronic LCMV (Lymphocytic Choriomeningitis Virus) model.[20] Alternatively, KLRG1$^+$ Tconv may take on a suppressive function as has been noted in vitro,[21] or as a result of high CD39 expression as seen with exhausted CD8 T cells in cancer.[22] However, it remains possible KLRG1$^+$ Tregs are a passive byproduct and quantifiable marker of an alternative dominant suppressive factor in the TME. For future use of KLRG1$^+$ Tconv as biomarkers of ICB response, additional studies are needed to resolve our observed discrepancy in KLRG1 RNA and protein levels in human tumor-infiltrating CD4 T cells. While this phenomenon is likely explained by the sparsity of single cell data, it is possible that stabilization of surface KLRG1 by its ligands—E-cadherin, N-cadherin, or R-cadherin[23 24]—in the TME is a mechanism by which this discrepancy occurs, however, additional investigation is needed. Finally, while KLRG1$^+$ Tregs are known to be highly immunosuppressive,[18 25] our data suggest it is a Helios$^-$ subset of KLRG1$^+$ Tregs that may be uniquely functionally relevant, as they are a highly consistent marker of tumor burden, progression, and ICB response in our models. Whether these Tregs are peripherally induced from KLRG1$^+$ Tconv, and if these cells exhibit unique functional characteristics from Helios$^+$KLRG1$^+$ Tregs are open questions for further study.

In total, this study calls for future investigation into KLRG1$^+$ CD4 T cell subsets as potential targets of—or putative biomarkers for—cancer immunotherapy. Though our data warrant mechanistic follow-up and additional validation in clinical specimens, the concordance of our observations with others in various other ectopic and autochthonous models suggests these cell types may be generalizable across tumor types in both mice and humans.[13 25] Furthermore, our findings are proof of concept that a longitudinal high-parameter spectral flow cytometry approach can be applied to additional model systems and time points to extract novel targets and/or biomarkers from dynamic 'temporal atlases' of antitumor immunity. It is likely these and related approaches will be critical in better understanding the complex, dynamic interactions that shape the TME, and ultimately lead to more effective utilization of immunotherapy in the clinic.

Author affiliations
[1]Department of Medicine, Division of Hematology and Oncology, Columbia University Irving Medical Center, New York, New York, USA
[2]Department of Immunology, Mayo Clinic Arizona, Scottsdale, Arizona, USA
[3]Columbia Center for Translational Immunology, Columbia University Irving Medical Center, New York, New York, USA
[4]Department of Urology, Mayo Clinic Arizona, Scottsdale, Arizona, USA
[5]Department of Molecular Pathology and Therapeutics, Columbia University Irving Medical Center, New York, New York, USA
[6]Department of Radiation Oncology, Columbia University Irving Medical Center, New York, New York, USA
[7]Department of Systems Biology, Columbia University Irving Medical Center, New York, New York, USA
[8]Janssen Research and Development, Janssen Pharmaceuticals, Spring House, Pennsylvania, USA
[9]Herbert Irving Comprehensive Cancer Center, Columbia University Irving Medical Center, New York, New York, USA
[10]Department of Urology, Columbia University Irving Medical Center, New York, New York, USA
[11]Columbia University Vagelos College of Physicians and Surgeons, New York, New York, USA

Twitter Casey R Ager @caseyager and Benjamin Izar @bizarMD

Acknowledgements We thank Dr. Cory Abate-Shen at Columbia University for kindly sharing the NPK-C1 cell line.

Contributors CRA: conceptualization, methodology, validation, formal analysis, investigation, data curation, writing, visualization. MZ: formal analysis, visualization. MC: investigation. SB: investigation. ST: formal analysis, visualization. AO: software, formal analysis, visualization. CJ: investigation. MR: conceptualization, writing—review. JCM: writing—editing. PM: investigation. CS: supervision. CGD: supervision, funding acquisition. MCD: resources, supervision, funding acquisition. BI: conceptualization, resources, writing—editing, supervision, project administration, funding acquisition.

Funding CRA was supported by the NIH grants UL1TR001873 and TL1TR001875. This research was funded in part through the NIH/NCI Cancer Center Support Grant P30CA013696, a Prostate Cancer Foundation Challenge Award (CGD/MCD). BI is supported by NIH grants, R37CA258829, R21CA263381, R01CA280414 and R01CA266446, and the Pershing Square Sohn Cancer Research Alliance Award, the Burroughs Wellcome Fund Career Award for Medical Scientists; a Tara Miller Melanoma Research Alliance Young Investigator Award; the Louis V. Gerstner, Jr. Scholars Program (Columbia University); and the V Foundation Scholars Award.

Competing interests BI has received consulting fees from Volastra Therapeutics, Merck, AstraZeneca and Janssen Pharmaceuticals and has received research funding to Columbia University from Alkermes, Arcus Biosciences, Checkmate Pharmaceuticals, Compugen, Immunocore, and Synthekine. CGD is a coinventor on patents licensed from JHU to BMS and Janssen, has served as a paid consultant to AZ Medimmune, BMS, Pfizer, Roche, Sanofi Aventis, Genentech, Merck, and Janssen, has received sponsored research funding to his institution from BMS IIoN and Janssen, and is a current employee of Janssen.

Patient consent for publication Not applicable.

Ethics approval All experiments and procedures for this study were approved by the Institutional Animal Care and Use Committees (IACUC) at Columbia University (AABI2613) and Mayo Clinic (A00007127).

Provenance and peer review Not commissioned; externally peer reviewed.

Data availability statement Data are available on reasonable request. Flow cytometry datasets generated in this study are available on reasonable request. Single cell RNA sequencing data analyzed in this study are previously published; our analyses are available on reasonable request.

ORCID iDs
Casey R Ager http://orcid.org/0000-0003-0507-700X
Benjamin Izar http://orcid.org/0000-0003-2379-6702

REFERENCES

1 Alban TJ, Chan TA. Immunotherapy biomarkers: the long and winding road. *Nat Rev Clin Oncol* 2021;18:323–4.
2 Marabelle A, Fakih M, Lopez J, *et al*. Association of tumour mutational burden with outcomes in patients with advanced solid tumours treated with pembrolizumab: prospective biomarker analysis of the multicohort, open-label, phase 2 KEYNOTE-158 study. *Lancet Oncol* 2020;21:1353–65.
3 Samstein RM, Lee C-H, Shoushtari AN, *et al*. Tumor mutational load predicts survival after immunotherapy across multiple cancer types. *Nat Genet* 2019;51:202–6.
4 Le DT, Durham JN, Smith KN, *et al*. Mismatch repair deficiency predicts response of solid tumors to PD-1 blockade. *Science* 2017;357:409–13.
5 Reck M, Rodríguez-Abreu D, Robinson AG, *et al*. Pembrolizumab versus chemotherapy for PD-L1-positive non-small-cell lung cancer. *N Engl J Med* 2016;375:1823–33.
6 Angell HK, Bruni D, Barrett JC, *et al*. The immunoscore: colon cancer and beyond. *Clin Cancer Res* 2020;26:332–9.
7 Havel JJ, Chowell D, Chan TA. The evolving landscape of biomarkers for checkpoint inhibitor Immunotherapy. *Nat Rev Cancer* 2019;19:133–50.
8 Fridman WH, Meylan M, Petitprez F, *et al*. B cells and tertiary lymphoid structures as determinants of tumour immune contexture and clinical outcome. *Nat Rev Clin Oncol* 2022;19:441–57.
9 Ager CR, Obradovic AZ, Arriaga JM, *et al*. Longitudinal immune profiling reveals unique myeloid and T-cell phenotypes associated with spontaneous immunoediting in a prostate tumor model. *Cancer Immunol Res* 2021;9:529–41.
10 Aytes A, Mitrofanova A, Kinkade CW, *et al*. Etv4 promotes metastasis in response to activation of Pi3-kinase and Ras signaling in a mouse model of advanced prostate cancer. *Proc Natl Acad Sci U S A* 2013;110:E3506–15.
11 Braun DA, Street K, Burke KP, *et al*. Progressive immune dysfunction with advancing disease stage in renal cell carcinoma. *Cancer Cell* 2021;39:632–48.
12 Obradovic A, Chowdhury N, Haake SM, *et al*. Single-cell protein activity analysis identifies recurrence-associated renal tumor macrophages. *Cell* 2021;184:2988–3005.
13 Li A, Herbst RH, Canner D, *et al*. IL-33 signaling alters regulatory T cell diversity in support of tumor development. *Cell Rep* 2019;29:2998–3008.
14 Alvarez MJ, Shen Y, Giorgi FM, *et al*. Functional characterization of somatic mutations in cancer using network-based inference of protein activity. *Nat Genet* 2016;48:838–47.
15 Borys SM, Bag AK, Brossay L, *et al*. The Yin and Yang of targeting KLRG1(+) Tregs and effector cells. *Front Immunol* 2022;13.
16 Curran MA, Geiger TL, Montalvo W, *et al*. Systemic 4-1BB activation induces a novel T cell phenotype driven by high expression of eomesodermin. *J Exp Med* 2013;210:743–55.
17 Schiering C, Krausgruber T, Chomka A, *et al*. The alarmin IL-33 promotes regulatory T-cell function in the intestine. *Nature* 2014;513:564–8.
18 Cheng G, Yuan X, Tsai MS, *et al*. IL-2 receptor signaling is essential for the development of KLRG1+ terminally differentiated T regulatory cells. *J Immunol* 2012;189:1780–91.
19 Joshi NS, Akama-Garren EH, Lu Y, *et al*. Regulatory T cells in tumor-associated tertiary lymphoid structures suppress anti-tumor T cell responses. *Immunity* 2015;43:579–90.
20 Daniel B, Yost KE, Hsiung S, *et al*. Divergent clonal differentiation trajectories of T cell exhaustion. *Nat Immunol* 2022;23:1614–27.
21 Vignali PDA, DePeaux K, Watson MJ, *et al*. Hypoxia drives CD39-dependent Suppressor function in exhausted T cells to limit antitumor immunity. *Nat Immunol* 2023;24:267–79.
22 Vignali P, DePeaux K, Watson M, *et al*. 679 tumor hypoxia drives suppressor function in exhausted T cells limiting antitumor immunity. *J Immunother Cancer* 2021;9:A707.
23 Tata A, Dodard G, Fugère C, *et al*. Combination blockade of KLRG1 and PD-1 promotes immune control of local and disseminated cancers. *Oncoimmunology* 2021;10:1933808.
24 Greenberg SA, Kong SW, Thompson E, *et al*. Co-inhibitory T cell receptor Klrg1: human cancer expression and efficacy of neutralization in murine cancer models. *Oncotarget* 2019;10:1399–406.
25 Adeegbe DO, Liu S, Hattersley MM, *et al*. BET bromodomain inhibition cooperates with PD-1 blockade to facilitate antitumor response in Kras-mutant non-small cell lung cancer. *Cancer Immunol Res* 2018;6:1234–45.